Optical fiber-based laser remote sensor for airborne measurement of wind velocity and turbulence

Scott M. Spuler,* Dirk Richter, Michael P. Spowart, and Kathrin Rieken

National Center for Atmospheric Research, Earth Observing Laboratory,
P.O. Box 3000, Boulder, Colorado 80307-3000, USA

*Corresponding author: spuler@ucar.edu

Received 7 October 2010; revised 3 December 2010; accepted 24 December 2010;
posted 10 January 2011 (Doc. ID 136178); published 15 February 2011

We discuss an optical fiber-based continuous-wave coherent laser system for measuring the wind speed in undisturbed air ahead of an aircraft. The operational principles of the instrument are described, and estimates of performance are presented. The instrument is demonstrated as a single line of sight, and data from the inaugural test flight of August 2010 is presented. The system was successfully operated under various atmospheric conditions, including cloud and clear air up to 12 km (40, 300 ft). © 2011 Optical Society of America

OCIS codes: 280.3340, 120.0280, 010.3640, 010.3920, 010.7060, 280.7250.

1. Introduction

Accurate assessment of wind speed and direction from an in-flight aircraft is essential for many areas of experimental research. Obtaining accurate air velocity measurements by means of *in situ* sensors is onerous mainly as a consequence of flow distortion around the fuselage. The only feasible way of calibrating air velocity sensors on aircraft is by flight maneuvers, which limit the achievable accuracy. Therefore, it is problematic to accurately measure vertical air velocity fluctuations due to their small magnitude while, for example, a few tenths of meters per second are necessary for eddy flux measurements.

The National Center for Atmospheric Research [(NCAR), Colo., USA] operates a Gulfstream V (GV) aircraft for atmospheric research. On this aircraft, wind velocity is obtained from differential pressure sensors on the surface of the aircraft nose radome. Asymmetry of the radome is expected to result in significant velocity errors under certain conditions. Some improvement would be expected if the pressure sensors were mounted on a boom that extended at least a fuselage in diameter from the nose of the aircraft where the flow distortion is reduced. Nevertheless, this approach remains susceptible to the accuracy limitations of all immersion sensing techniques while potentially introducing errors from boom flexing. Remote sensing of wind velocity ahead of the distortion effects of the aircraft is a more desirable approach.

Optical remote sensing of wind velocity from aircraft can offer the following advantages: (i) measurement in undisturbed air with minimal flow distortion, (ii) ability to measure vertical wind shear, (iii) operation without a nose boom, (iv) operation in clouds, and (v) an absolute measurement independent of flight maneuvers and atmospheric conditions. In this regard, optical remote sensing can also be used synergistically with *in situ* measurements. The laser remote sensor can provide an absolute standard for improved calibration of the *in situ* measurements while, in turn, the pressure sensors can be used to fill in measurement gaps in the laser remote sensor, e.g., when operating in air with no appreciable aerosol concentrations.

The first deployment of an airborne laser Doppler velocimeter was in 1971 by Muñioz *et al.* [1], followed in 1987 by Keeler *et al.* [2] and Kristensen and Lenschow [3] who coined the term "laser air motion

0003-6935/11/060842-10$15.00/0

sensor" (LAMS). These seminal papers describe the limitations of immersion sensing techniques, the potential of laser remote sensing, and present theory and results from systems that utilized CO_2 lasers at 10.6 μm. The advent of fiber-based components has made it substantially more simple to implement a LAMS on an aircraft platform. An optical fiber-based LAMS has the potential to provide a much-needed and long-desired air velocity measurement that will provide valuable information about air motion in the vicinity of the aircraft as well as enable the continuous calibration of a radome gust probe. The opportunity to measure wind velocity remotely using laser technology offers significant improvements in accuracy and response time that will benefit many areas of research. For example, more accurate horizontal wind measurements will allow measurement of horizontal divergence and vorticity even in fairly quiescent conditions.

The LAMS described in this paper is in the first stage of development with a goal of providing measurement of three air velocity components from an aircraft more accurately than existing systems. The instrument—flown as a single line of sight to measure true airspeed—had multiple successful flights on board the NCAR GV aircraft throughout August and September of 2010. This paper provides a description of the instrument design and configuration on the aircraft as well as initial results of the first test flight. A more detailed analysis of the instrument performance from all of the flights is underway.

2. Principles of Operation and Estimate of Performance

The instrument described herein falls in the general category of Doppler laser remote sensing. It is a coaxial laser system that utilizes optical heterodyning of the signal backscatter from atmospheric aerosols. Principles of operation of such instruments are well described by Sonnenschein and Horrigan [4]. To estimate the performance of the instrument, we begin by calculating the number of photons transmitted per second given by

$$n_T = \frac{P_T}{h\nu}, \tag{1}$$

where P_T is the transmitted power, h is the Planck constant, and ν is the laser frequency.

The instrument follows the all-fiber design of Karlsson *et al.* [5], where the end of the fiber was polished at a shallow angle so that a small percentage of the transmitted beam was reflected upon exit. The reflection forms a local oscillator (LO), with a reference photon rate given as n_{ref}, which is a small percentage of the transmitted photon rate (e.g., for this work, the fiber was angle polished to have a −37 dB reflection). A fraction of the transmitted photons is backscattered from aerosols present in the atmosphere. These photons are Doppler shifted—due to the radial velocity of the scatterers—so they interfere constructively and destructively with the reference photons at the detector. The resultant frequency is proportional to the laser wavelength and the wind velocity along the laser line of sight:

$$v = -\frac{\lambda f_D}{2}, \tag{2}$$

where v is the velocity along the laser line of sight, λ is the wavelength of the seed laser, and f_D is the measured frequency.

The combined photon rate incident on the detector surface is converted to an electric current given by [4]

$$i_s^2 = n_T n_{\mathrm{ref}} \beta_\pi \eta^2 G^2 e^2 \pi r_t^2 \times \int_0^\infty \left(L^2 \left[1 + \left(\frac{\pi r_t}{\lambda L} \right)^2 \left(1 - \frac{L}{f} \right)^2 \right] \right)^{-1} \mathrm{d}L, \tag{3}$$

where β_π is the aerosol backscatter coefficient, η is the detector quantum efficiency, G is the internal gain of the detector (for an InGaAs pin $G \sim 1$), e is the electron charge, λ is the laser wavelength, L is the distance from the transmitter telescope of radius r_t, and f is the range to the laser focus. Carrying out the integration of Eq. (3), we obtain

$$i_s^2 = n_T n_{\mathrm{ref}} \beta_\pi \eta^2 G^2 e^2 \lambda \left[\frac{\pi}{2} + a\tan\left(\frac{\pi r_t^2}{\lambda f} \right) \right]. \tag{4}$$

If the system is shot noise limited, then the noise from the detector can be given as

$$i_n^2 = 2\eta G^2 e^2 n_{\mathrm{ref}} B, \tag{5}$$

where B is the receiver bandwidth or the width of the spectral feature of interest.

From these equations, it follows that the electrical current or voltage (i.e., typical output from an optical detector) signal-to-noise ratio (SNR) can be expressed as

$$\mathrm{SNR} = \left[\frac{\eta P_T \beta_\pi \lambda}{2Bh\nu} \left(\frac{\pi}{2} + a\tan\left(\frac{\pi r_t^2}{\lambda f} \right) \right) \right]^{1/2}, \tag{6}$$

which is the square root of the electrical power SNR that uses the ratio of the *squared* currents.

As evident in Eq. (6), the system performance is dependent on the aerosol backscatter coefficient, β_π, and therefore on the presence of aerosols in the atmosphere. To estimate β_π for our performance models, we primarily used a data set obtained during airborne lidar campaigns that included low-, mid-, and high-latitude observations taken over the Atlantic ocean from 1988 to 1990 [6]. The backscatter coefficients from this observational data set were scaled from the 10.6 wavelength to 1.56 μm by the relationship discussed in Srivastava *et al.* [7]. The scaled median and lower decile values were used for our performance estimate calculations. The statistical distribution of aerosol backscatter versus altitude

was in general agreement with observational data [7] with the lower decile of backscatter coefficients approaching $3 \times 10^{-10}\,\mathrm{m^{-1}sr^{-1}}$ for altitudes above 5 km. The low backscatter coefficients at high altitudes required the LAMS to be designed with high optical power and significant signal averaging.

Figure 1 shows the estimated performance of the instrument signal-to-noise versus altitude. The range between the median and lower decile backscatter coefficients are shown for two cases—without averaging and with averaging. The air at the lowest altitudes—within the atmospheric boundary layer—typically has higher backscatter coefficients, and the instrument could operate with little averaging. But the rapid decrease in backscatter coefficients into the midtroposphere (>5 km altitude) requires the system to utilize high optical power and substantial averaging with high-speed data acquisition. The performance estimate curves presented in Fig. 1 are for a transmitted laser power of 3 W and 200,000 spectra averaged for an equivalent data rate of 1 Hz. Based on our atmospheric aerosol backscatter statistical model and assuming shot noise limited performance, the LAMS should be able to provide consistent measurement of air velocity up to ~5 km altitude and frequently to even higher altitudes.

3. Design

To demonstrate instrument capability, we constructed an optical fiber-based continuous-wave laser remote sensor for use on the NCAR GV aircraft. The optical setup is shown in Fig. 2. The instrument was designed to have most of the components mounted within the aircraft cabin. This included the seed distributed feedback fiber laser (NKT Photonics BasiK Module C15) with a center vacuum wavelength of 1560 nm, 5 W single-mode fiber amplifier (Nufern PSFA-1560-VV-5W-Y-Z), amplified InGaAs PIN diode detector (Menlo FPD310), analog and digital signal processing electronics, and data acquisition computer. This configuration was useful because it reduced the size and weight of the wing pod and kept most of the sensitive components in a more benign operational environment.

Unlike similar optical fiber-based laser velocimeters used for ground-based applications (e.g., Karlsson *et al.* [5]) this configuration required that the laser and optical head were separated by ~20 m. The onset of stimulated Brillouin scattering (SBS) can be a significant source of noise with this fiber length at high laser power levels. Therefore, a unique configuration of optical fiber types and optical circulator location was required to achieve optimal performance.

Testing at power levels of 1.3 W revealed a significant increase in the backscattered noise level with increased fiber length. With a standard single mode fiber type, SMF-28, an increase of 5.5 dBm was measured (at the frequency peak of 8 MHz) with a fiber length increase from 1 to 19 m. Substituting a

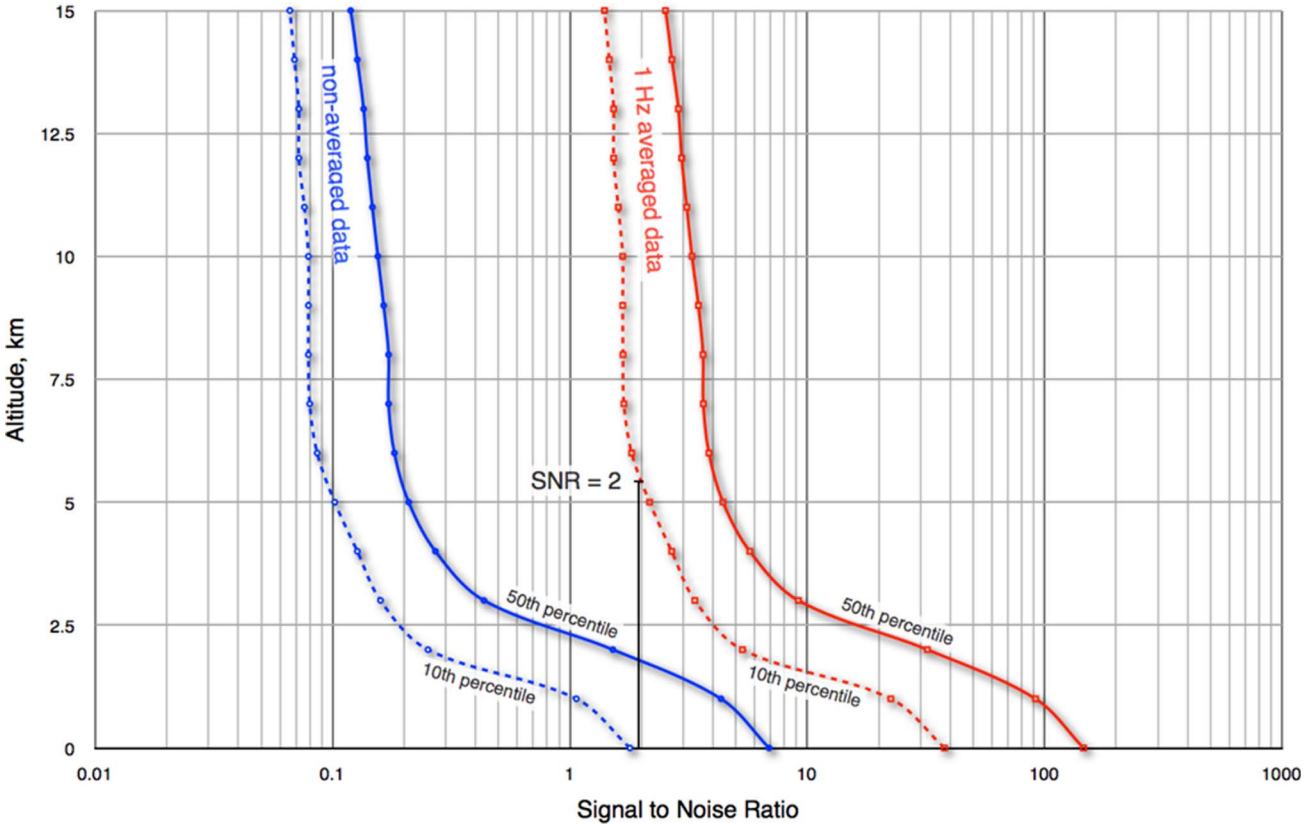

Fig. 1. (Color online) Predicted instrument signal to noise as a function of aircraft altitude. Inputs included 3 W transmitted optical power and 200,000 spectra averaged—equivalent to 1 Hz data rate.

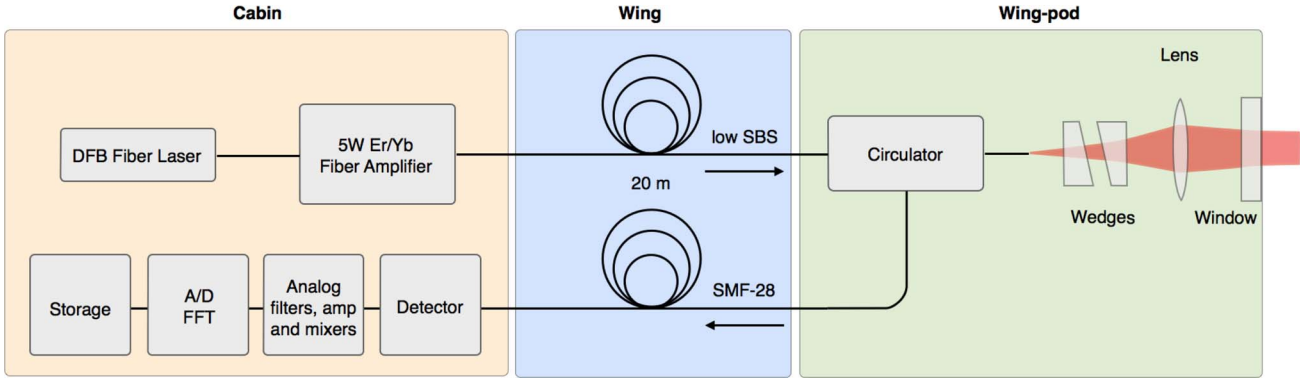

Fig. 2. (Color online) Optical setup of the LAMS. Component location on the aircraft is indicated by the large shaded boxes. Note that the end of the fiber was polished at a shallow angle so that a small percentage of the transmitted beam was reflected upon exit. The reflection forms the LO, and for this work, the fiber was angle polished to have a −37 dB reflection.

passive low-SBS fiber (Neolight PA111-001) for the SMF-28 fiber suppressed the backscatter noise level; however, it was still 2.0 dBm above the short fiber length baseline. To allow for an increase in power, we chose to use a pair of single-mode optical fibers to connect components in the cabin with those in the wing pod. The passive low-SBS fiber was used for the outgoing laser light, and the standard SMF-28 fiber was used for the low-power return. Experimentation was required to optimize the fusion splice between the SMF-28 fiber-based components (e.g., laser and circulator) and the low-SBS fiber. We were able to achieve a splice loss of 0.1 dB. In this configuration there was no measurable increase in the backscattered noise level with initial laser power levels up to 4.75 W—equivalent to 3 W of transmitted power.

The design trade-off for this low-noise configuration required the 5 W optical power handling, polarization-independent, circulator (OFR OC-3-1550) to be mounted in the wing pod. This component couples single-mode fibers to a chain of several small free-space optics. The fiber optic coupling requires tight positional tolerances, and, therefore, it can be sensitive to misalignment at excessive temperature ranges. This necessitated thermal stabilization because the wing-pod temperature could range from +35 C to −65 C. Even when temperature stabilized, there was a risk with this component within the aircraft wing pod. Interruption in electrical power to the wing for an extended period of time could lead to substantial degradation in instrument performance. Therefore, it would be advantageous to substitute a more athermalized component should one become available, e.g., a high-power handling optical fiber-based circulator.

Figure 3 shows a detailed view of the wing pod used to test the instrument. The fiber pair from the wing was routed into a standard instrumentation wing canister where they were spliced to the circulator. The output fiber of the circulator entered a sealed optical bench (1 atm of dry nitrogen) held within the nose cone. The bare fiber end was securely held in place on a v groove mounted on a three-axis translation stage used to optimize the beam quality at the focus. A pair of prisms was used to compensate for the beam refraction at the angled fiber end. The laser was focused at a distance of 30 m from the canister utilizing a 50 mm diameter, 200 mm focal length lens. The distance was selected to be sufficiently removed from the aircraft flow distortion, yet close enough that the coherence between the remotely measured velocity and the velocity at the point where scalar variables are measured is still high. The $1/e^2$ beam diameter was estimated to be 38 mm at the lens. Therefore, the sample length at 30 m in front of the wing pod was approximately 2.5 m [defined as $(8/\pi)(f/d)^2\lambda$, which is the FWHM of the telescope gain pattern]. As shown in Fig. 3, a nose cone covered the optical bench. The front of the cone contained a 50 mm diameter fused silica window. The window mount had temperature controlled rod heaters installed around the perimeter to keep the window free from ice.

The instrument aircraft configuration is shown in Fig. 4. The laser line of sight was roughly aligned with the direction of flight. The GV aircraft generally flies with a 3° pitch up, and the laser was pointed approximately 3° down. This allowed for a near-direct comparison between the true airspeed derived from the standard aircraft pressure sensors and the LAMS. Changes in the laser line of sight angle due to aircraft and wing motion were measured with a combined global positioning system (GPS) and inertial navigation system (INS) unit attached to the same strut as the LAMS wing pod. The two pressure-based *in situ* airspeed sensors shown in Fig. 4 were used for true airspeed intercomparisons with the LAMS and discussed in the experimental section of this paper. The avionics Pitot-static tubes were used to derive true airspeed at 1 Hz and the combined fuselage Pitot tube and static port on the side of the plane were used to derive 50 Hz true airspeeds. The Pitot tubes used for the GV avionics measure the total true airspeed regardless of alignment for small angles.

The instrument had a laser wavelength of 1560.0 nm; therefore, Doppler frequencies of 100–200 and 200–300 MHz correlate to true airspeeds of 78–156 and 156–234 m/s respectively—as given by Eq. (2). The signal from the detector was split into

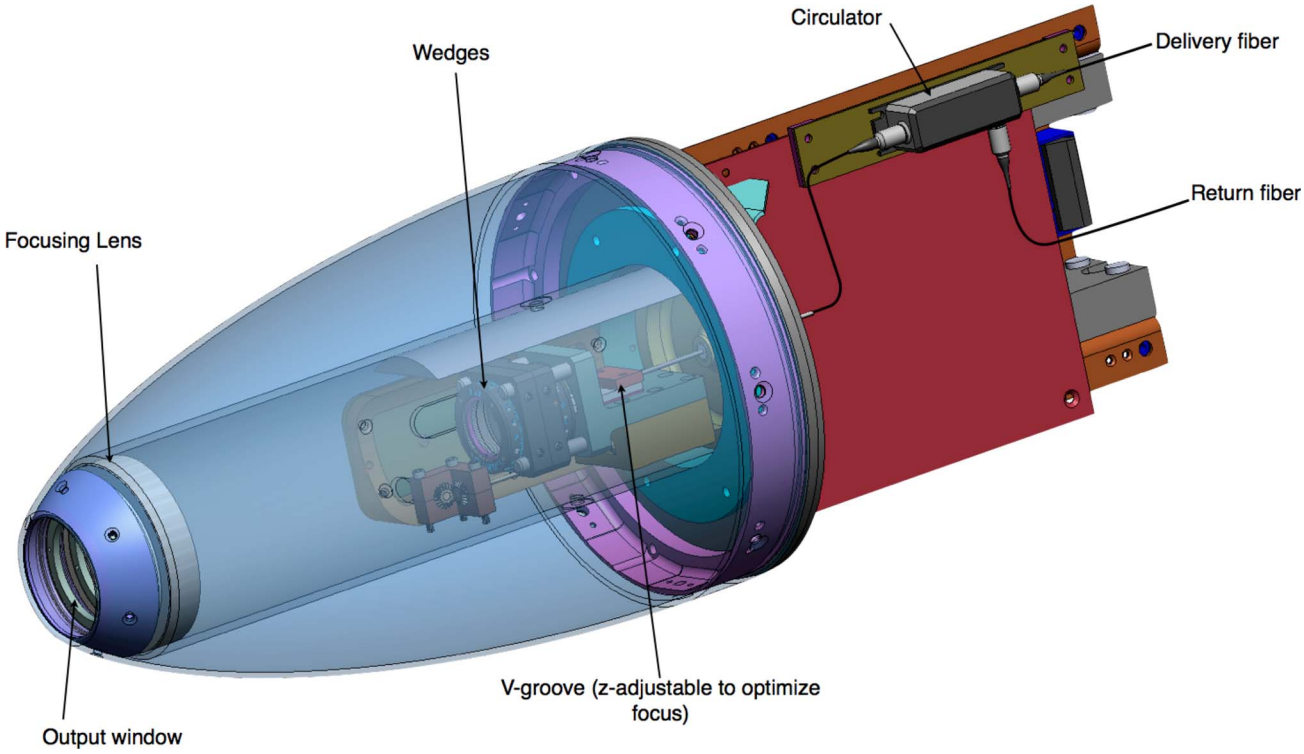

Fig. 3. (Color online) Detail of the prototype LAMS wing pod used for demonstration and validation.

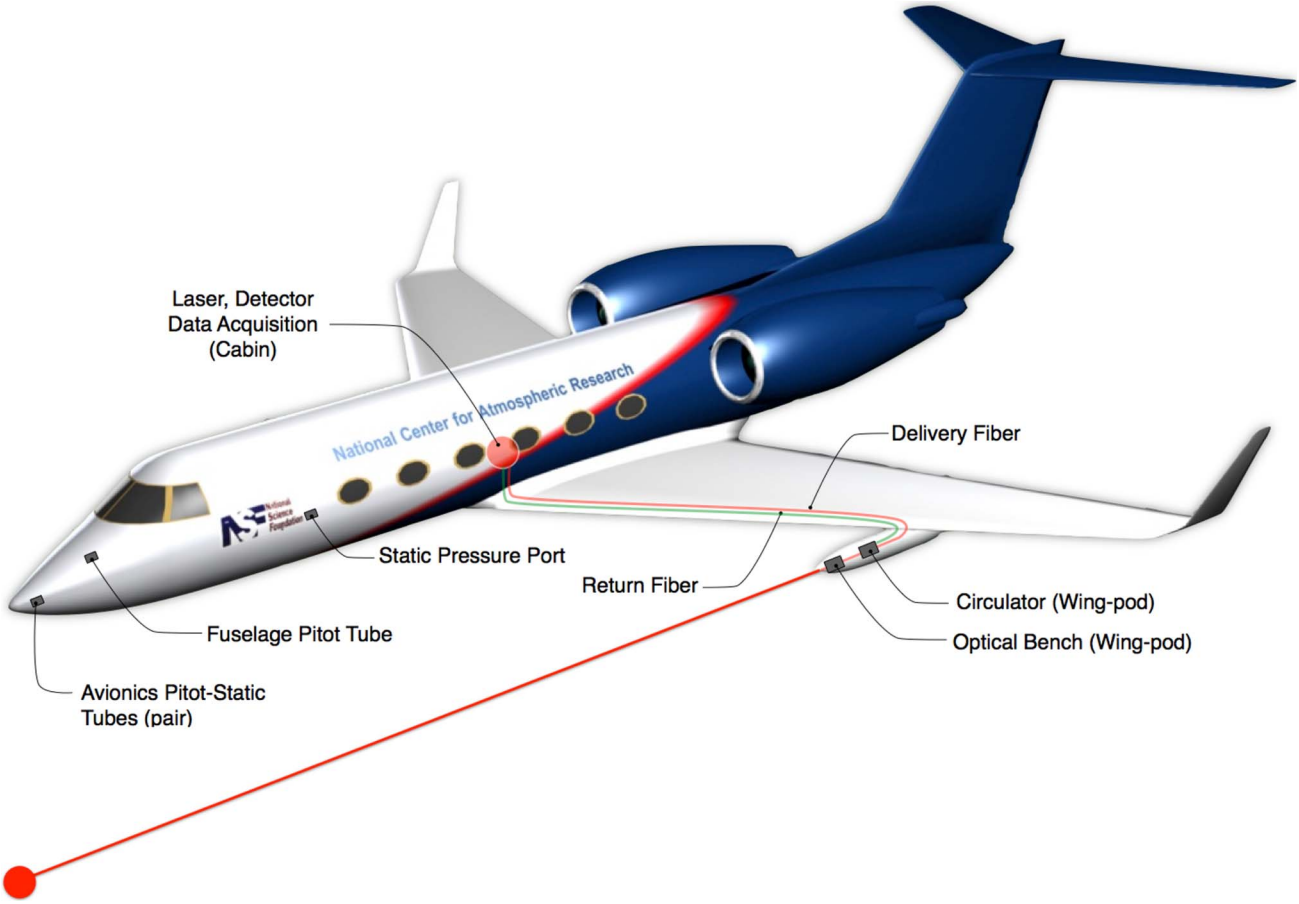

Fig. 4. (Color online) LAMS installation for the NCAR GV. The laser and detector are cabin mounted, with fibers running in the wing connecting them to a small optical bench that was used to focus the laser at a fixed location about 16 m in front of the nose of the aircraft.

two—one high-pass filtered at 100 MHz and the other high-pass filtered at 200 MHz. A switch triggered at an aircraft true airspeed of 156 m/s was used to select the appropriate high-pass filtered signal. This analog signal was amplified 53 dB and simultaneously low-pass filtered at 350 MHz via the amplifier frequency response. The bandpass filtered signal was sent into a mixer stage. For true airspeeds below 156 m/s the signal was mixed with a 100 MHz LO, whereas, for speeds exceeding 156 m/s, a 200 MHz LO was used. The resultant mixed and bandpass-filtered signal was analog-to-digital converted at a rate 200×10^6 samples per second with 14 bit resolution. Doppler frequencies outside of the bandpass range, although attenuated, were aliased and folded into the data acquisition. A field-programmable gate array (FPGA) was used to compute 1024-point fast Fourier transforms in pipeline mode—at a data rate of ~200 MHz. The resultant 512-point frequency histogram had four possible wind speed ranges—78–0 m/s (folded), 78–156 m/s, 156–234 m/s, and 312–234 m/s (folded)—and a spectral point spacing equivalent to 0.15 m/s. These spectra were averaged on the FPGA and output at 100 Hz to a data storage system.

Using postprocessing algorithms, the baseline fluctuations of the spectral histogram were removed in two steps. The spectrum was first high-pass filtered, and then the remaining baseline was removed using a principal component analysis and linear regression. A Gaussian function was convolved with the baseline-flattened spectra to isolate the peak frequency. The spectral position of the peak of the Gaussian fit was converted to all four possible speeds. The actual speed was selected by minimizing the difference between these possible speeds and the true airspeed measured by the flight avionics. This approach generally worked well; however, it led to some ambiguity at the sampling discontinuities (i.e., frequencies exactly at 100 and 200 MHz). As a final data processing step, spectral peaks with a SNR below 1 were discarded to remove low-confidence wind estimates.

4. Experimental Results

The initial test flight occurred on 3 August 2010. The 1 Hz data from this flight is shown in Fig. 5. The upper panel of the figure shows the true airspeed from the LAMS, the derived true airspeed from the Avionics Pitot-static tubes (variable TASA) and the fuselage pressure system, which measures differences in a static Pitot tube at the nose of the plane, and a static pressure port on the side (variable TASF). It is difficult to see the different lines in the plot because they all agree quite well with one another at this scale (note that the middle panel allows one to see the differences). The aircraft altitude is shown on the right y axis. As mentioned previously, the laser was configured to point straight ahead during normal flight operations. Therefore, the pointing angle corrections required to compensate for differences in the laser line of sight and the direction of the aircraft were small (in general the correction was <0.1 m/s). Changes in the instrument pointing angle from any wing motion were corrected using 5 Hz data from the GPS/INS.

As shown in the upper panel of Fig. 5, following takeoff, the LAMS began to measure airspeeds above 25 m/s. The slower speeds were attenuated by the bandpass of the data acquisition system. Throughout the ascent, the instrument SNR was sufficient to provide near continuous measurement of wind speed up to an altitude of 11 km at 21:00 UTC. At an altitude of 12.3 km, from 21:10 to 21:40 UTC, the instrument was able to intermittently measure winds speeds within relatively clear air with low aerosol concentrations. This marginal SNR was expected, based on our performance estimate, for air with backscatter coefficients less than 7×10^{-10} m^{-1}sr^{-1}. During the descent, from 21:45 to 22:35 UTC, the instrument was able to measure winds speeds with regularity.

The differences in the LAMS-measured TAS and the derived TAS from the pressure sensors are shown in the middle panel of Fig. 5. At aircraft speeds <200 m/s the differences between the LAMS and the TAS calculated from avionics and fuselage pressure sensors are generally less than 1 m/s. At aircraft speeds over 200 m/s, differences greater than 1 m/s are evident. At most aircraft speeds, there was an offset of about 1 m/s between the two pressure-based measurements. "Speed run" flight maneuvers were performed at different altitudes to more fully investigate potential errors in the pressure sensors. These maneuvers are segments where the pilots varied the speed of the aircraft while maintaining a level altitude and are evident in the upper panel of Fig. 5 as rapid changes in speed that occur at 20:13 UTC (3.2 km), 20:35 UTC (3.0 km) 21:15 UTC (12.5 km), and 21:51 UTC (6.7 km). During the final speed run, the LAMS-TASF differences indicate swings of -1.25 m/s to $+0.75$ m/s. As these deviations are not seen in the LAMS-TASA difference, it is likely that this is due to errors in the correction factors applied to the TASF data. This illustrates the limitation in accuracy of the current pressure-difference velocity measurement system.

The LAMS SNR is plotted on the bottom panel of Fig. 5 for the duration of the test flight. Although we did not have a direct measurement of the backscatter coefficient at this wavelength, because aerosol backscatter is a function of aerosol concentration, diameter, shape, and type, we can get a rough sense of instrument performance by comparing with the aerosol number density. The total aerosol concentration for particles in the size range of 0.1 to 3 μm in diameter is plotted on the right y axis as the square root of the total particles/cm^3 [the instrument SNR should scale with the square root of aerosol backscatter coefficient, as shown in Eq. (6)]. The plot shows good general agreement between the LAMS SNR and the square root of the concentration for these aerosol sizes. Based on performance in the relatively clean air at 12.5 km, and noting the aforementioned

caveats about unknown particle shape and type, we can roughly estimate that the instrument limit of detection is ~2 particles/cm^3 for this aerosol size range.

To gain some understanding of instrument precision and potential vibration effects, a section of test flight data from 21:57 to 22:03 UTC was selected for further analysis. This time series was selected because it was a period of relatively high-altitude flight—level at 6.7 km with constant airspeed around 220 m/s. As can be seen from the middle panel of Fig. 5, the difference between the *in situ* derived TAS and the LAMS TAS, there was an offset of about 1 m/s and 0.5 m/s from the avionics and fuselage pressure measurements, respectively. The Allan variance, also known as the two-sample variance, is routinely calculated for laser spectrometers to determine instrument stability times and identify systematic errors, such as frequency drift [8]. The Allan variance was calculated for this time period on the difference data (e.g., LAMS TAS—TASA) in order to remove atmospheric turbulence effects. An Allan plot of the TAS difference data is shown as Fig. 6. As shown in the figure, the 1 s variance for the LAMS-TASA data is 0.0027 $(m/s)^2$, which indicates that the LAMS precision is ≤ 0.052 m/s. Additionally, the slope of the line follows the expected slope

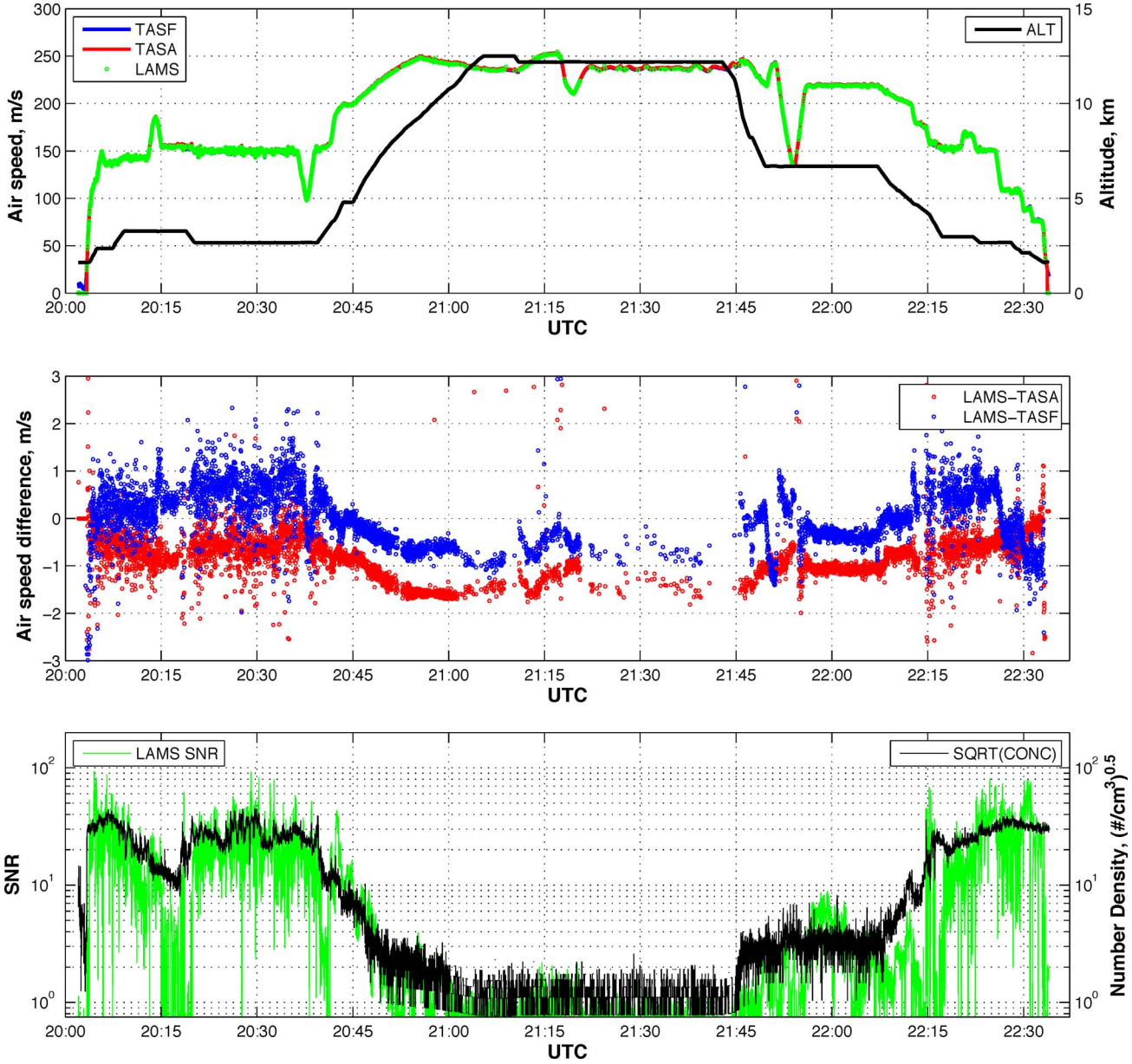

Fig. 5. (Color online) This figure shows the 1 Hz data for the test flight on 3 August 2010. The top panel shows true airspeed derived from avionics Pitot-static tubes, TASA, fuselage static Pitot tube and static pressure port, TASF, and the LAMS. The aircraft altitude (in kilometers) is shown on the right y axis. The middle panel is a plot of the difference between LAMS and the two *in situ* derived true airspeeds. The bottom panel is a plot of the LAMS SNR on the left axis and the square root of the aerosol concentration, SQRT(CONC), on the right y axis.

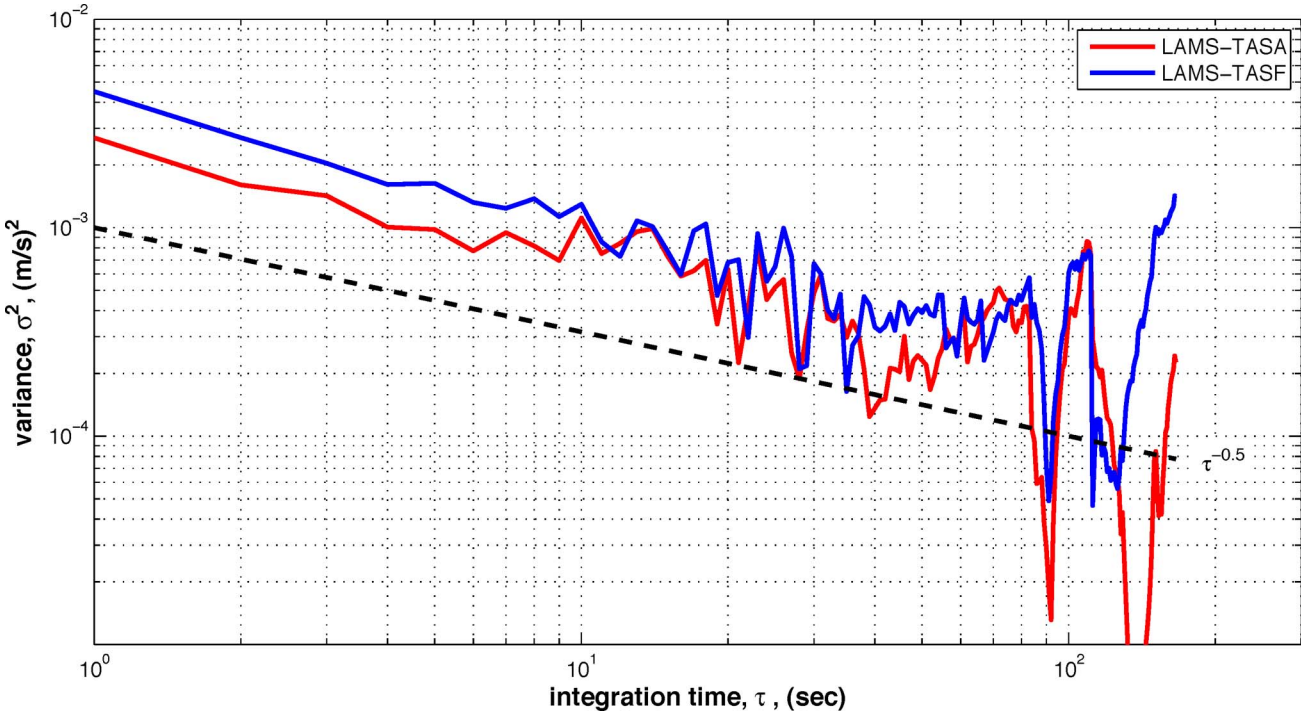

Fig. 6. (Color online) Allan variance plot of the TAS difference data from time series from 21:57 to 22:03 UTC. The slope of the dashed line is fixed at $\tau^{-0.5}$.

(i.e., noise decreases at the rate of $\tau^{-0.5}$), which implies that there are no systematic sources of noise (e.g., vibration effects) under these flight conditions.

A time series of the measured true airspeed at 50 Hz is shown in Fig. 7. The 6 min segment from a low-altitude boundary layer portion of the flight (20:20 to 20:26 UTC) demonstrates the typical high-temporal resolution performance of the instrument in regions with considerable atmospheric turbulence. For this time series, the LAMS true airspeed was in general agreement with the fuselage-derived true airspeed. There were, however, deviations up to 2 m/s on short time scales. The laser data led the pressure data in time, as expected, because the system was focused ~16 m in front of the nose of the aircraft. A cross-covariance of the time series indicated a ~0.1 s lag—equivalent to an 18 m separation in the sample locations at the average measured true airspeed. The 2 m difference is likely due to the delay in response time from the tubing length of the pressure system. To verify the response of the LAMS to turbulence, it is helpful to plot the velocity spectra of the time series measurement, as shown in Fig. 8. The turbulence data follow the expected Kolmogorov inertial subrange −5/3 slope [9] up to the 25 Hz limit imposed by the data rate. The frequency response of the TASF is not as good and begins to deviate from the expected slope above 1 s. Therefore, any difference on short time scales can likely be attributed to errors in the TASF at high frequencies. A more

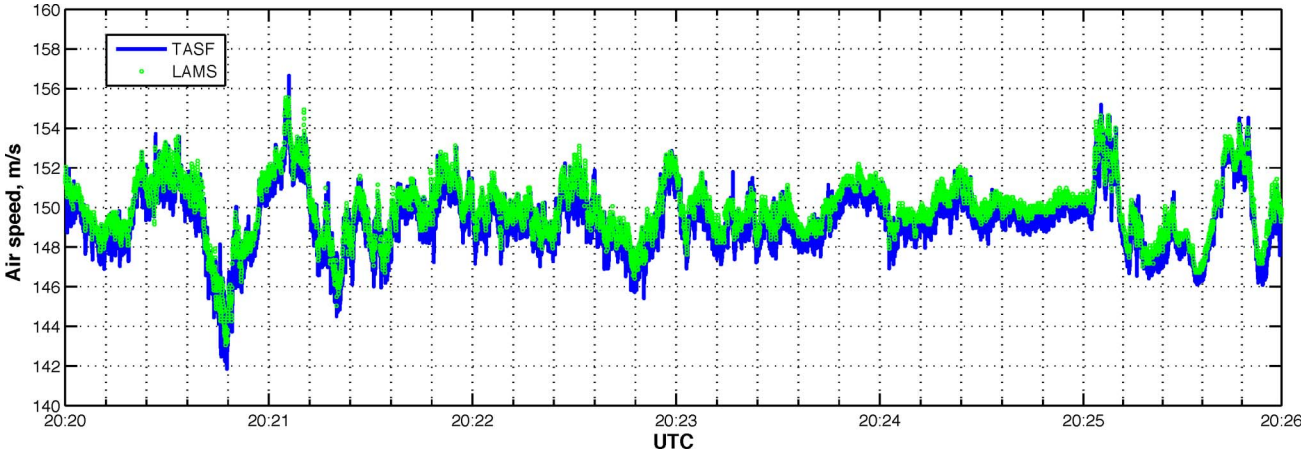

Fig. 7. (Color online) Sample high-rate time series of the true airspeed from the LAMS and the fuselage pressure differential sensor at low altitude. The 6 min segment was at a level altitude of 2660 m.

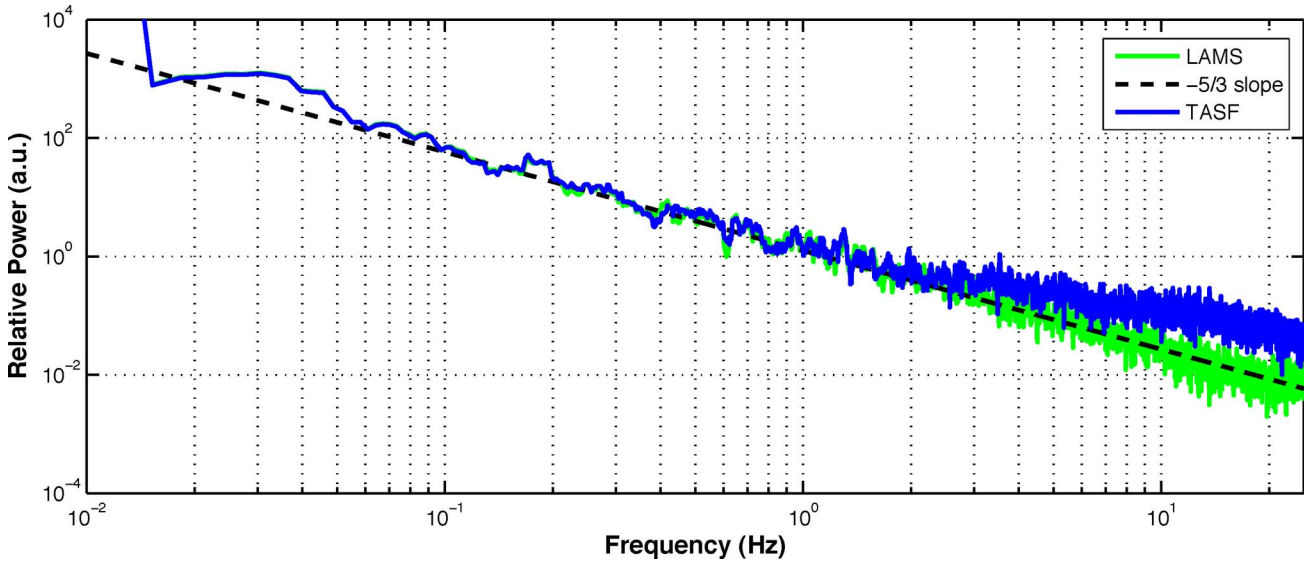

Fig. 8. (Color online) Velocity power spectrum of the time series of the LAMS and the fuselage differential pressure system from the time period 20:20 to 20.26 UTC. The slope of the dashed line indicates Kolmogorov's –5/3 frequency dependence in the inertial subrange.

complete analysis of the turbulent section of the test flights is still to be evaluated. At this time we can conclude that the LAMS instrument was able to consistently measure wind speeds at a 50 Hz data rate in the lower portion of the atmosphere with the appropriate frequency response.

The LAMS instrument was operated on 14 flights throughout August and September of 2010. Of these, three were test flights based out of Broomfield Colorado, USA, one was a ferry flight, and ten were research flights as part of the Pre-Depression Investigation of Cloud Systems in the Tropics field campaign based out of St. Croix in the U.S. Virgin Islands. Instrument performance was similar on all of these flights. The Colorado-based test flights, and the ferry flights, contained a series of flight maneuvers that should help more fully define the capabilities of the instrument. During three of the research flights the aircraft passed through sections of high ice-water content air that adversely affected the *in situ* true airspeed measurements and plugged temperature inlets. The LAMS data should prove valuable in understanding these events. A detailed study of all the flights is currently underway.

5. Conclusions

The development of an optical fiber-based LAMS began as an effort to resolve flow distortion issues around the NCAR GV aircraft radome. Information gathered during the first test flights indicated there is a limited temporal response and accuracy issues with the *in situ* measurements that are likely caused by inaccurate flow distortion correction factors. The LAMS has been demonstrated to provide low-altitude wind speeds at a data rate of 50 Hz. High altitude measurement of winds speeds at 1 s update rates were also obtained—albeit with less consistency in "clear air" regions. The test flights successfully demonstrated the proof of concept and confirm the potential of such an instrument to make a valuable contribution to the aircraft observational measurement community. Detailed analysis of the complete data set from all test flights is ongoing, while the next-generation instrument is under development. The main objective of the new instrument is to provide three-dimensional wind measurements. It is being designed with similar construction to the single-axis unit but with three angled beams emitting from the wing pod. It may include improved noise reduction techniques and employ more temperature-resilient circulators.

This development was funded by the National Center for Atmospheric Research and the Earth Observing Laboratory. The authors would like to thank Larry Murphy for technical support; Donald Lenschow, Richard Friesen, and William Cooper for atmospheric science guidance; Christopher Webster for software engineering support; Lars Rippe and Ethan Gutman for help with the postprocessing algorithm; and Stephen Rauenbuehler for the mechanical engineering design. The National Center for Atmospheric Research is sponsored by the National Science Foundation.

References

1. R. M. Muñioz, H. W. Mocker, and L. Koehler, "Airborne laser Doppler velocimeter," Appl. Opt. **13**, 2890–2898 (1974).
2. R. Keeler, R. Serafin, R. Schwiesow, D. Lenschow, J. M. Vaughan, and A. Woodfield, "An airborne laser air motion sensing system. part I: concept and preliminary experiment," J. Atmos. Ocean. Technol. **4**, 113–127 (1987).
3. L. Kristensen and D. Lenschow, "An airborne laser air motion sensing system. part II: design criteria and measurement possibilities," J. Atmos. Ocean. Technol. **4**, 128–138 (1987).
4. C. M. Sonnenschein and F. A. Horrigan, "Signal-to-noise relationships for coaxial systems that heterodyne backscatter from the atmosphere," Appl. Opt. **10**, 1600–1604 (1971).
5. C. J. Karlsson, F. A. Olsson, D. Letalick, and M. Harris, "All-fiber multifunction continuous-wave coherent laser radar at

1.55 μm for range, speed, vibration, and wind measurements," Appl. Opt. **39**, 3716–3726 (2000).
6. J. M. Vaughan, D. W. Brown, C. Nash, S. B. Alejandaro, and G. G. Koenig, "Atlantic atmospheric aerosol studies 2. compendium of airborne backscatter measurements at 10.6 μm," J. Geophys. Res. **100**, 1043–1065 (1995).
7. V. Srivastava, J. Rothermel, A. D. Clarke, J. D. Spinhirne, R. T. Menzies, D. R. Cutten, M. A. Jarzembski, D. A. Bowdle, and E. W. McCaul, "Wavelength dependence of backscatter by use of aerosol microphysics and lidar data sets: application to 2.1 μm wavelength for space-based and airborne lidars," Appl. Opt. **40**, 4759–4769 (2001).
8. P. Werle, "Accuracy and precision of laser spectrometers for trace gas sensing in the presence of optical fringes and atmospheric turbulence," Appl. Phys. B (to be published).
9. R. B. Stull, *An Introduction to Boundary Layer Meteorology* (Kluwer Academic, 1988).